We are IntechOpen,
the world's leading publisher of
Open Access books
Built by scientists, for scientists

6,900
Open access books available

186,000
International authors and editors

200M
Downloads

Our authors are among the

154
Countries delivered to

TOP 1%
most cited scientists

12.2%
Contributors from top 500 universities

CLARIVATE ANALYTICS
BOOK CITATION INDEX
INDEXED

WEB OF SCIENCE™

Selection of our books indexed in the Book Citation Index
in Web of Science™ Core Collection (BKCI)

Interested in publishing with us?
Contact book.department@intechopen.com

Chapter

Synthesis Methods and Crystallization of MOFs

Yitong Han, Hong Yang and Xinwen Guo

Abstract

Metal-organic frameworks (MOFs) are a class of porous crystalline materials constructed of metal centres with organic linkers, creating one-, two-, or three-dimensional well-organized frameworks with very high surface areas. The study of MOFs has become one of the research hot spots in many fields, owing to the broad potential applications projected for these materials in various areas. It is well recognized that synthesis strategies dictate the structure and thus the properties and performance of the resulted MOFs. This chapter provides a comprehensive up-to-date overview on the modulated synthesis strategies for MOFs. The ability to control crystal morphology and size by a number of modulated synthesis methods is illustrated by the zirconium-terephthalate-based MOF, the UiO-66, and a number of other MOFs.

Keywords: metal-organic frameworks, synthesis method, crystallization, crystal morphology and size control

1. Introduction

Porous materials are a class of solid compounds with an ordered and/or disordered pore structure, high pore volume, and large surface area. These combined with some of their unique chemistries make them a unique class of chemical and engineering materials. Over the past three decades, porous materials have become one of the research hot spots in the fields of chemistry, physics, and materials science and engineering. The diversity in the pore orientation and dimensionality, combined with the multiplicity in pore shapes and sizes, makes the porous materials highly interested and widely studied. The IUPAC defines the porous materials based on the pore dimensions and classifies them into the microporous materials with pore dimension less than 2 nm, mesoporous materials with pore dimension ranging from 2 to 50 nm, and macroporous materials with pores larger than 50 nm [1].

Porous materials have shown great application values in some traditional industries, such as the oil and gas processing, industrial catalysis, adsorption/separation, and fine chemical industries [2–5]. In more recent decade, they are also being recognized and explored in the research fields of water treatment, sustained release of drugs, and fuel cells, to name a few [6, 7].

Among all porous materials, zeolites are perhaps the most famous microporous materials. In the frameworks of the zeolites, different numbers of TO_4 tetrahedral primary structure units connect together to form shared apexes, which enable the creation of the interconnected secondary structure units of various shapes and the formation of the microporous zeolite structure. The "T" in the TO_4 tetrahedrons is usually silicon, aluminum, and phosphorus. Chemically, zeolites have adjustable acidity, in addition to

their excellent pore channel selectivity and hydrothermal stability. These support the high research value of zeolites in industrial applications such as exchange, adsorption/separation, and petroleum processing. However, the inorganic nature of zeolites limits their adjustability in chemical properties and designability in pore structures and sizes, which restrict the further development and applications of zeolites [2].

For decades, there have been research efforts trying to integrate various metal centres and functional organic molecules into porous structures for the modulation of physical and chemical properties. This effort has resulted in the development of a novel type of hybrid porous crystalline materials formed by the coordination of inorganic metal centres and organic linkers in the 1990s. This new class of porous materials is most commonly known as metal–organic frameworks (MOFs), although they are also sometimes known as porous coordination polymers (PCPs) or inorganic-organic hybrid materials [8–10]. Ever since their discovery, MOFs have received significant attention from scientists, engineers, and technologists due to their versatilities in structures and chemistries. Since the synthesis of MOFs directly influences the crystallization of the MOF structure, thus dictates its properties and functional performance, extensive work and thousands of research papers have continually emerged focusing on the development of synthesis methods.

The aim of this chapter is to provide an up-to-date overview on the synthesis methods of MOFs reported so far, with the objective to provide empirical guidance for developing synthesis strategy for MOF materials targeting specific properties and functionalities. We draw on our own extensive experiences on modulated synthesis of the UiO-66 MOF material to demonstrate how the crystal morphology and size can be controlled by different modulated synthesis methods, mechanisms of crystallization, and effect of metal doping on MOF crystals during synthesis.

2. Structure and applications of MOFs

As stated in the introduction, MOFs are a unique class of hybrid porous crystalline materials and have been widely studied over the past two decades for their inherent structure design flexibility and potential applications [11].

The structures of MOFs are constructed by self-assembly between the "nodes" of metal-containing secondary building units (SBUs) and the "bridges" of organic linkers, creating one-, two-, or three-dimensional well-organized network structures with very high pore volumes and surface areas. The framework topologies and pore structures and sizes of MOFs can be designed via selecting various metal centres and organic linkers. Their chemical properties can be modified by chemical functionalization of linkers and post modifications [12–14].

MOFs have extended the chemistry of the porous materials from inorganic to inorganic-organic hybrid. This compositional diversity, combined with the structural diversity, gives them unique properties and functionalities. MOFs are thus a class of highly attractive porous materials for a broad range of applications, including in gas adsorption/separation [15–18], luminescence and sensing [19–22], catalysis [23–25], and others [26–29].

3. Synthesis methods and crystallization of MOFs

3.1 Overview of synthesis methods for MOFs

At their discovery, the method for synthesis of MOFs is solvothermal. Typically, metal precursors and organic linkers are dissolved in solvent and placed in a closed

reaction vessel for the formation and self-assembly of MOF crystals. The common solvents used include N,N-dimethylformamide (DMF), N,N-diethylformamide (DEF), methanol, ethanol, and acetonitrile. The synthesis temperature is generally below 220°C, and the crystallization time varies from several hours to several tens of days.

After more than two decades of research and development, great advances have been made in the synthesis of MOFs. New synthesis methods such as the electro-chemical, microwave-assisted, mechanochemical synthesis, microfluidic synthesis method, etc. have all been reported [30]. **Figure 1** summarizes the development timeline for the most common synthesis approaches of MOFs [30].

These diverse methods have enabled the synthesis of hundreds of new MOF structures since its first discovery. On top of this, as clearly stated in the principle of "structure dictates function" [31], having the ability to control and tailor the morphology and size and their chemical functionalization of MOF crystals is vital in delivering targeted properties and performances of the resulted MOF materials. This demands the development of more sophisticated synthesis strategies based on the understanding of mechanisms of crystallization occurred during synthesis. The following provides an overview on the currently developed modulated synthesis methods for morphology and size control of MOF crystals and doping to create hybrid MOF crystals.

3.2 Morphology and size control of MOF crystals

The synthesis of MOFs involves the process of crystallization during which the nucleation and growth of crystals occur. The nucleation and growth of MOF crystals involve the self-assembly between metal-oxygen clusters and organic link-ers. Understanding the influencing factors on the nucleation and growth of MOF crystals during their synthesis will enable accurate controlling of crystal morphol-ogy and size. The following discusses the morphology and size development of the MOF crystals during different modulated syntheses.

3.2.1 Deprotonation regulation synthesis

It is well documented that synthesis conditions, such as temperature, time, solvent type, and reactant concentrations, play important roles in the morphology and size of resulted MOF crystals.

For example, an NH_2-MIL-125(Ti) MOF material can be synthesized by a solvothermal method in a mixed solvent of DMF and methanol. **Figure 2** shows the SEM images of the NH_2-MIL-125(Ti) crystals synthesized with different reactant concentrations, as indicated by the total solvent volumes. By changing the total volume of the solvent alone while maintaining constant ratio between the DMF and methanol and amount of reactants, the morphology of the NH_2-MIL-125(Ti)
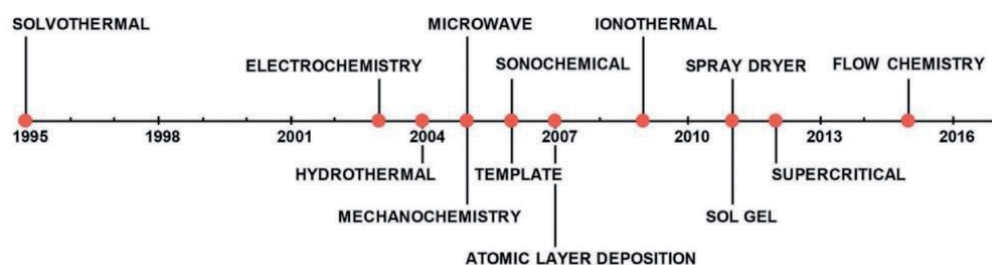

Figure 1.
Timeline of the most common synthesis approaches for MOFs [30].

crystals can be modified from circular plates to tetragons and octahedrons [32]. As the crystal morphology changes, the light absorption band of the NH$_2$-MIL-125(Ti) can be tuned from 480 to 533 nm, making it advantageous in photocatalytic applications.

It has been found that the reactant concentration has a significant effect on the deprotonation rate of the organic linkers during the synthesis of NH$_2$-MIL-125(Ti) crystals. The deprotonation rate plays a critical role in the nucleation and growth of the NH$_2$-MIL-125(Ti) crystals. Modulating crystal morphology and size of MOFs by changing the rate of deprotonation is called the deprotonation regulation synthesis [33].

3.2.2 Coordination modulation synthesis

Besides changing synthesis conditions, introducing additives during crystallization is another strategy of controlling the morphology and size of MOF crystals. The research lead by Kitagawa first reported the coordination modulation of carboxylic acid additives on the growth of [{Cu$_2$(ndc)$_2$(dabco)}$_n$] MOF crystals [34]. In this work, a specific amount of acetic acid is added in the crystallization mother liquor of the [{Cu$_2$(ndc)$_2$(dabco)}$_n$]. Acetic acid hinders the coordination
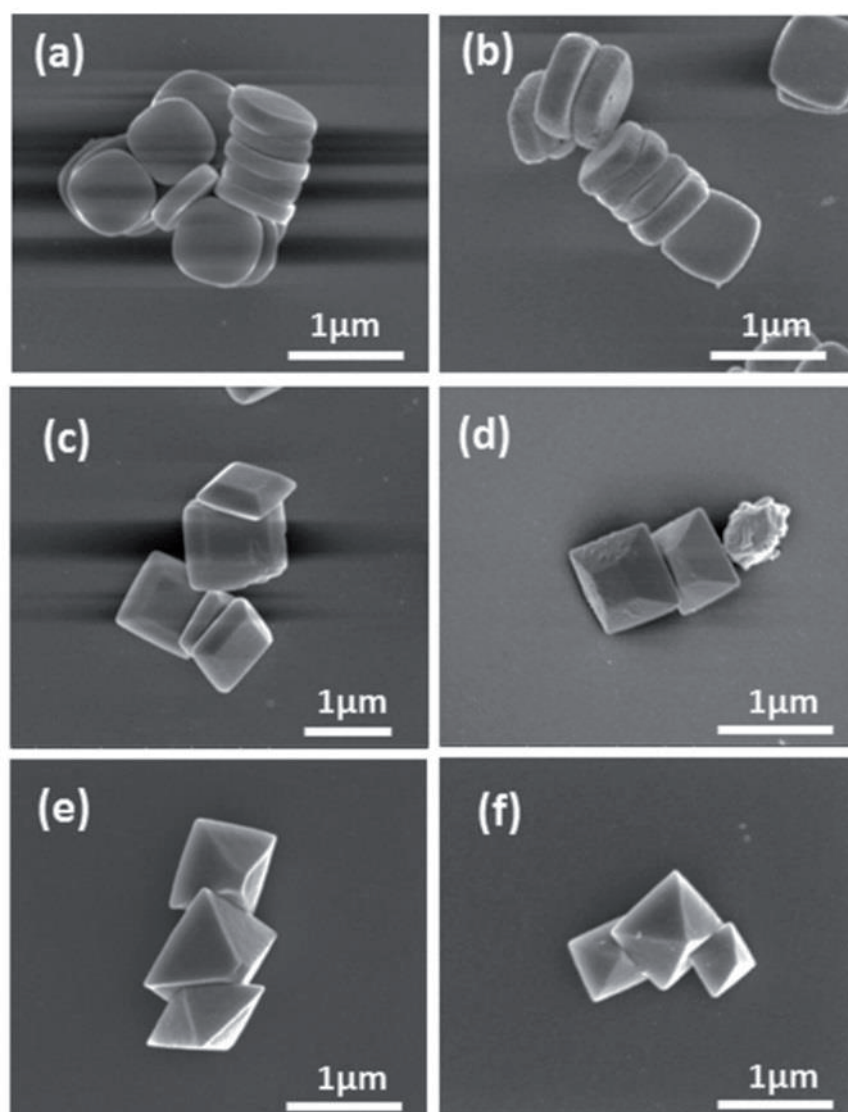
Figure 2.
SEM images of NH$_2$-MIL-125(Ti) crystals synthesized with different total solvent volumes of (a) 40 mL, (b) 30 mL, (c) 20 mL, (d) 15 mL, (e) 14 mL, and (f) 13.5 mL [32].

between metal clusters and organic linkers through selective coordination with the metal clusters. This influences the expansion of lattice structure and alters the growth of the $[\{Cu_2(ndc)_2(dabco)\}_n]$ crystals. **Figure 3** shows the nanocrystals of $[\{Cu_2(ndc)_2(dabco)\}_n]$ formed under the capping effect of acetic acid [34].

Subsequently, Kitagawa's group has also synthesized the HKUST-1 crystals using three kinds of monocarboxylic acid additives, the acetic acid, dodecanoic acid, and lauric acid under ultrasonic condition. **Figure 4** shows the effect of additive quantity on the morphology of the resulted HKUST-1 crystals. As seen, with the increased additive quantity, not only the size of the HKUST-1 crystals increases from tens of nanometres to several micrometres, the shape of the crystals also changes from cube to octahedron, truncated cube, and tetradecahedron, progressively [35, 36].

It has since been established that the coordination modulation which resulted from using the carboxylic acids has certain universality. It is shown to effectively control the crystal morphology and size of a number of MOFs, including $\{Cu_2(ndc)_2(dabco)\}_n$, HKUST-1, Zr-based MOFs, etc. The amount of the additive used ranges from 2 to 100 equimolar of the reactants. The carboxylic acid additives do not affect the crystal structure of the resulted MOFs.

3.2.3 Surfactant modulation synthesis

Some surfactants, such as the cetyltrimethylammonium bromide (CTAB) [37] and polyvinylpyrrolidone (PVDF) [38, 39], can also be used for the modulated synthesis of MOFs. In the crystallization of MOF crystals, the surfactant molecules can be selectively absorbed on one or more specific facets of the MOF crystals, thus hinder or alter their growth, and result in the modification of crystal morphology and size.

Take the hydrothermal synthesis of ZIF-67 MOF crystals as an example. As shown in **Figure 5**, by simply changing the amount of CTAB from 0.0025 to 0.025 wt%, a series of the ZIF-67 cubic or rhombic dodecahedron crystals with sizes ranging from ~150 nm to 1 μm can be produced [40]. Additionally, by carbonization of the resulted ZIF-67 crystals in N_2 flow, a series of Co-based porous carbon catalysts can be obtained. These Co-based porous carbon catalysts retain the
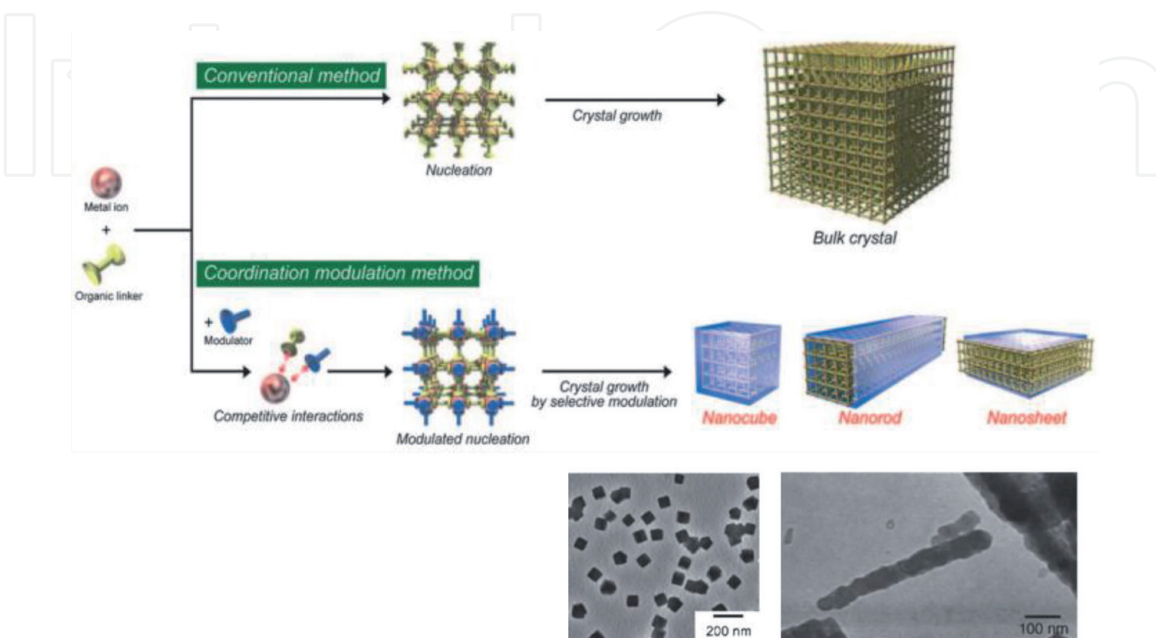

Figure 3.
Coordination modulation method for fabricating [{Cu₂(ndc)₂(dabco)}n] nanocrystals [34].
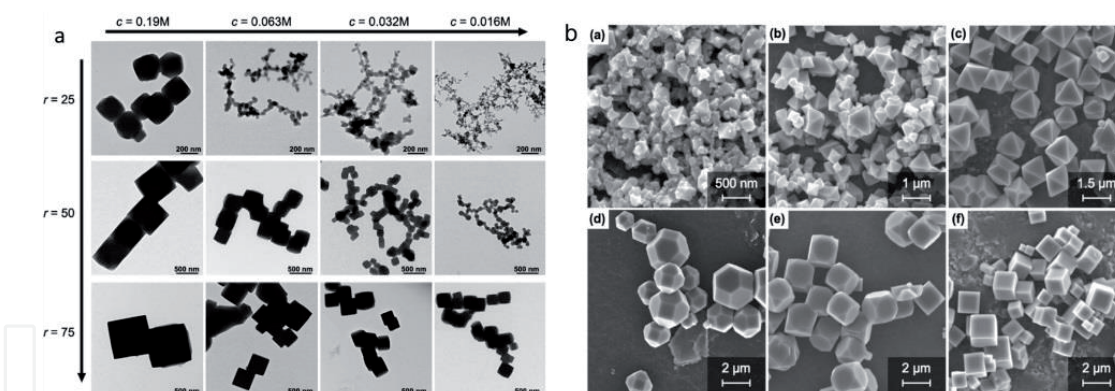
Figure 4.
(a) TEM images of the HKUST-1 crystals obtained with various concentrations of dodecanoic acid and H₃BTC; here C is the concentration of the H₃BTC and r is the molar ratio of dodecanoic acid to H₃BTC [35]. (b) SEM images of the HKUST-1 crystals obtained with different amounts of the lauric acid in mmol: (a) 0, (b) 2.34, (c) 4.75, (d) 7.13, (e) 9.5, and (f) 11.88 [36].
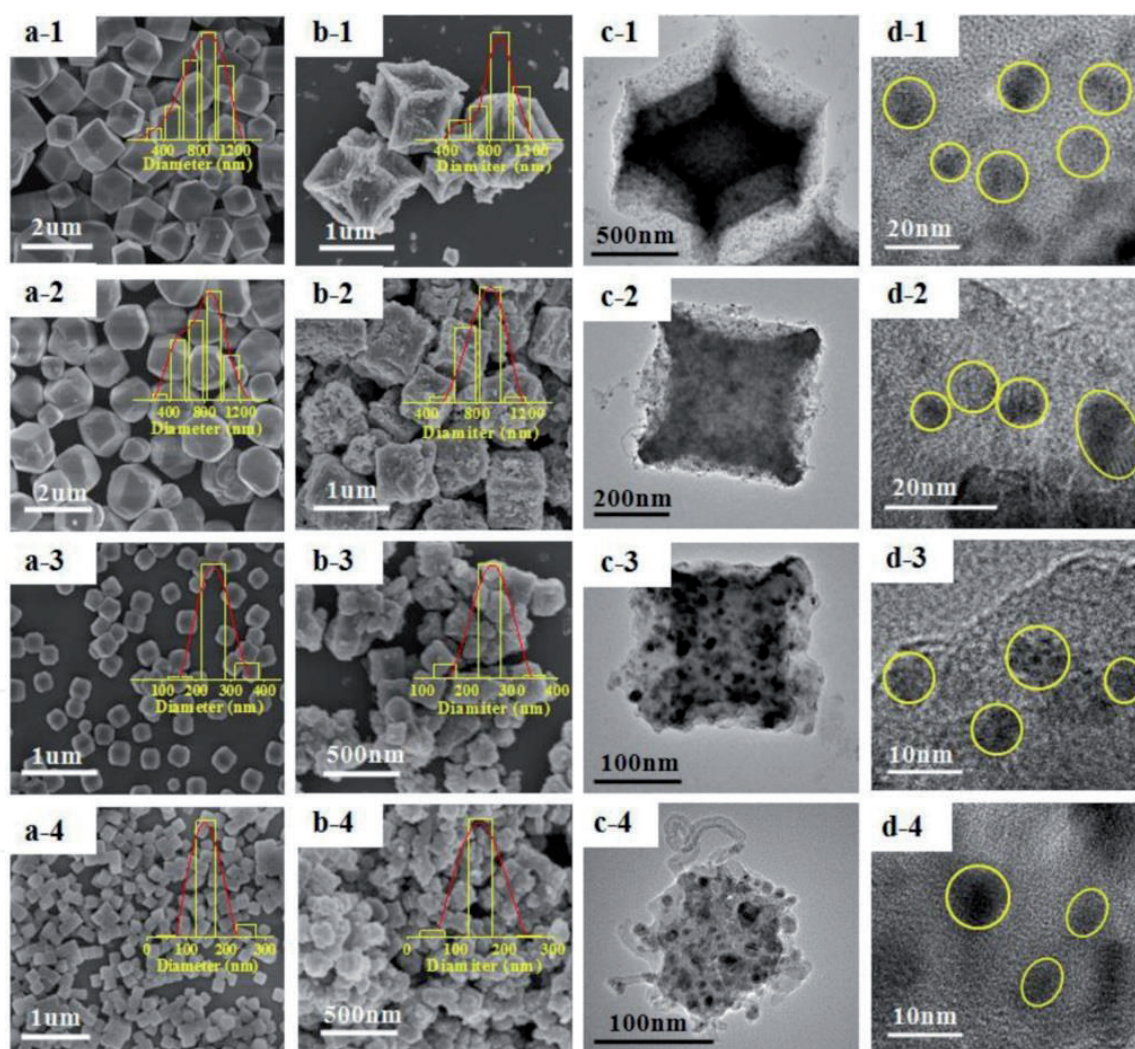

Figure 5.
ZIF-67 crystals synthesized with different amounts of the CTAB additive (1: 0, 2: 0.0025 wt%, 3: 0.01 wt%, and 4: 0.025 wt%). SEM and TEM images of (a) as-synthesized samples and (b–d) carbonized samples [40].

original shape of the ZIF-67 crystals and display an outstanding catalytic performance towards the CO_2 methanation at low temperatures.

It has also been reported that the addition of CTAB can modulate the crystal morphology and size of some other MOFs. **Figure 6** shows a number of such examples including IRMOFs [41, 42], HKUST-1 [43], and ZIF-8 [44].
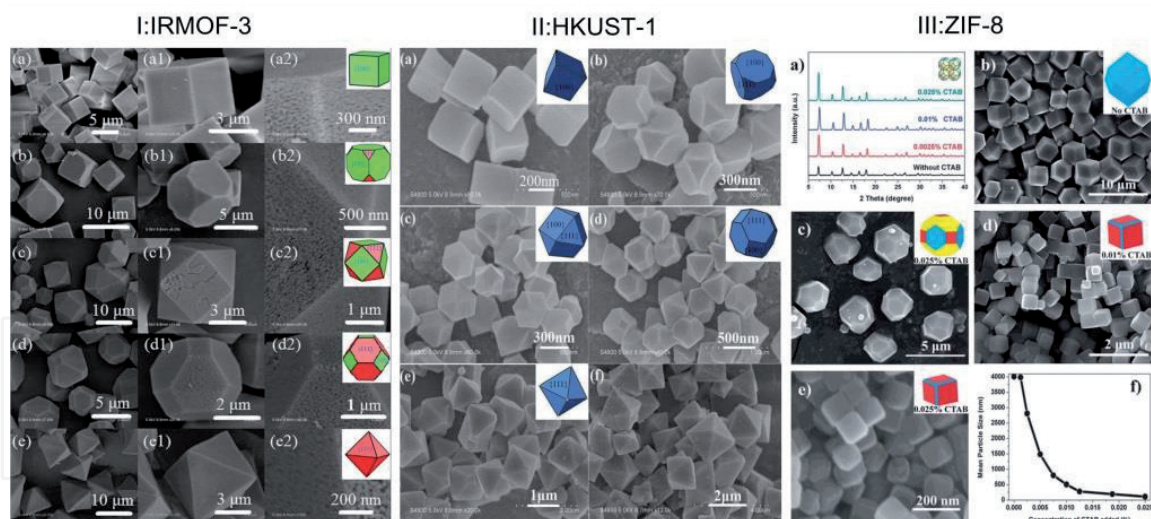
Figure 6.
The influence of CTAB additive on the crystal morphology and size of several MOFs. (I) SEM images of IRMOF-3 synthesized with different amounts of CTAB in mg: (a, a1, a2) 0, (b, b1, b2) 5, (c, c1, c2) 8, (d, d1, d2) 12, and (e, e1, e2) 15 [42]. (II) SEM images of HKUST-1 synthesized with different amounts of CTAB in M: (a) 0, (b) 0.005, (c) 0.01, (d) 0.05, (e) 0.1, and (f) 0.5 [43]. (III) (a) XRD patterns of ZIF-8; (b) ZIF-8 synthesized without CTAB; ZIF-8 synthesized with different amounts of CTAB in wt%: (c) 0.0025, (d) 0.010, and (e) 0.025; (f) mean particle size of ZIF-8 crystals versus the concentrations of CTAB added [44].

4. The UiO-66 MOF

As one of the most important MOFs, the Zr-BDC ($Zr_6O_4(OH)_4(CO_2)_{12}$) MOF, commonly known as the UiO-66, has been extensively studied due to its high porosity and excellent structural stability at high temperatures and pressures, and excellent stability in chemical (acidic/basic) aggressive environments. The framework of the UiO-66 is built on the $[Zr_6O_4(OH)_4]$ SBUs, each coordinated with 12 1,4-benzene-dicarboxylate (H_2BDC) linkers. **Figure 7** illustrates the crystal structure of the UiO-66. Its cubic structure is composed of octahedral cages close to 11 Å and tetrahedral cages close to 8 Å, and these cages are connected through narrow triangular windows close to 6 Å [45].

4.1 Modulated synthesis of UiO-66 crystals using carboxylic acids

The UiO-66 crystals are commonly synthesized via a solvothermal method at 110–130°C and allowed to crystallize for 24 h. Without modulation, the obtained UiO-66 crystals are usually agglomerates of small cube-like particles of 80–200 nm in size and with low crystallinity. These UiO-66 crystals show low porosity with the BET surface area below 1000 $m^2 g^{-1}$.

To improve the crystallinity of the UiO-66 crystals, carboxylic acid additives have been applied in the synthesis. Schaate et al. first studied the influence of benzoic acid and acetic acid on the crystal growth of the UiO-66 and other Zr-based MOFs [46]. They have found the UiO-66 crystals synthesized are octahedrons of several hundred nanometres in size, as shown in **Figure 8**. These crystals have a high crystallinity with the BET surface area of up to 1400 $m^2 g^{-1}$. Schaate et al. suggested that the addition of the carboxylic acid additives changes the original coordination equilibrium and thus the crystal growth rate during the crystallization of the UiO-66 crystals. There exists a competition between the coordination of the BDC linkers and carboxylic acid additives towards the Zr_6 clusters. This becomes an obstacle for the connection of the BDC linkers and Zr_6 clusters, shifting the original coordination equilibrium. This behaviour can be exploited as a way to modulate the morphology and size of the resulted MOF crystals.
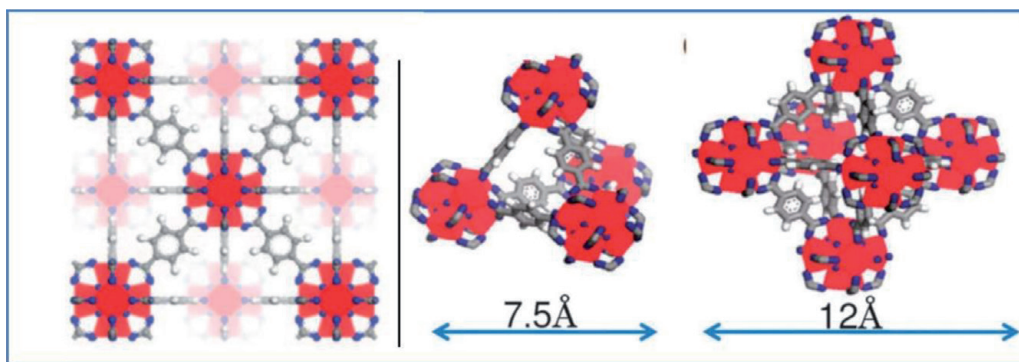
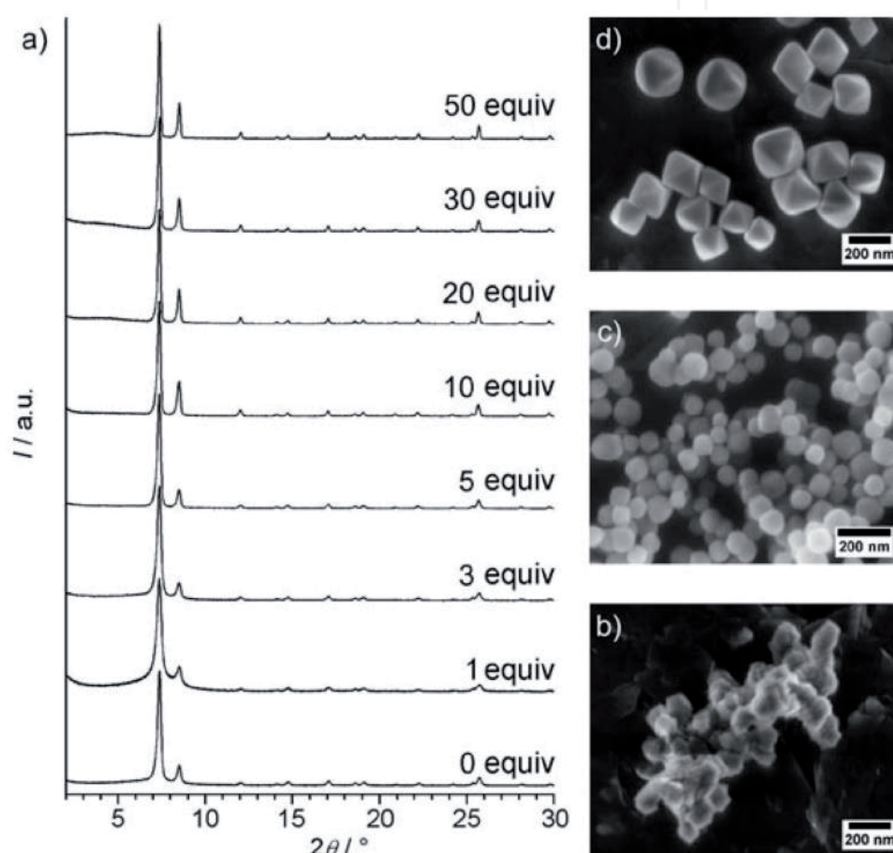**Figure 7.**
Schematic illustration of the UiO-66 structure [45].

Figure 8.
(a) XRD patterns and (b–d) SEM images of the UiO-66 crystals synthesized with different amounts of benzoic acid additive [46].

4.2 Modulated synthesis of UiO-66 crystals using HF

We have been working on precisely controlled synthesis of the UiO-66 and other MOFs with the aim to optimize their properties and extend their application potentials. We were the first to report a hydrofluoric acid (HF) modulated synthesis of the UiO-66 crystals from reactants $ZrCl_4$ and H_2BDC [47]. In the study, the amount of HF was varied from 1 eq. to 3 eq., where "eq." refers to the molar ratio of HF to $ZrCl_4$ in a synthesis batch. A control sample was also synthesized without the addition of HF but under otherwise identical conditions. **Figure 9** shows the SEM images of the UiO-66 crystals synthesized. As seen, the addition of the HF facilitates growth of the UiO-66 crystals with the mean size of the crystals increasing from ~150 nm to 7 μm with increased HF addition. By controlling the concentration of the reactants, the morphology of crystals changed from truncated cube to cuboctahedron.

To understand the impact of the HF additive, elemental mapping and ^{19}F NMR analysis of the resulted UiO-66 crystals were conducted.

Figure 10 shows the EDS mapping of the synthesized UiO-66 crystals. As seen, without the addition of HF, a small amount of Cl was detected in the crystals even after heat treatment up to 300°C. This somewhat unexpected observation of the Cl is believed to be resulted from structure defects in the synthesized UiO-66 crystals. It is known that the UiO-66 crystal structure contains defects in the form of missing linkers, which would result in an unsaturated framework. To compensate for this charge imbalance of the framework, negatively charged Cl ions (from the $ZrCl_4$ reactant) are "needed" to coordinate with the defective sites.

For the crystals synthesized with the addition of HF, EDS analysis of the crystals revealed noticeable F in the crystals, with no Cl observed. This indicates that, in the presence of stronger electronegative F, the F ions now coordinate to the linker defective sites instead of chlorine ions in the SBUs of the UiO-66 crystals.

This mechanism was further supported by the ^{19}F NMR spectra shown in **Figure 11**. As seen, the spectrum of 3F-UiO-66 heat-treated at 150°C (curve a) contains a strong signal of two partially overlapped peaks cantered at −155 ppm and −156 ppm. These peaks are assigned to the F bonded directly to Zr in the SBUs and the F physisorbed, respectively. When the 3F-UiO-66 is heat-treated at 300°C, as seen in curve (b), the peak at −155 ppm becomes stronger and narrower, whereas the peak at −156 ppm disappears. It indicates that F remains bonded to the Zr in the 3F-UiO-66 framework even after being heat-treated up to 300°C.

The thermostability of the UiO-66 crystals was enhanced after the introduction of fluorine in the framework structure. **Figure 12** shows the TGA curves of the UiO-66 crystals synthesized with different amounts of HF additive. The significant weight loss event observed at ~500°C represents the complete decomposition of the
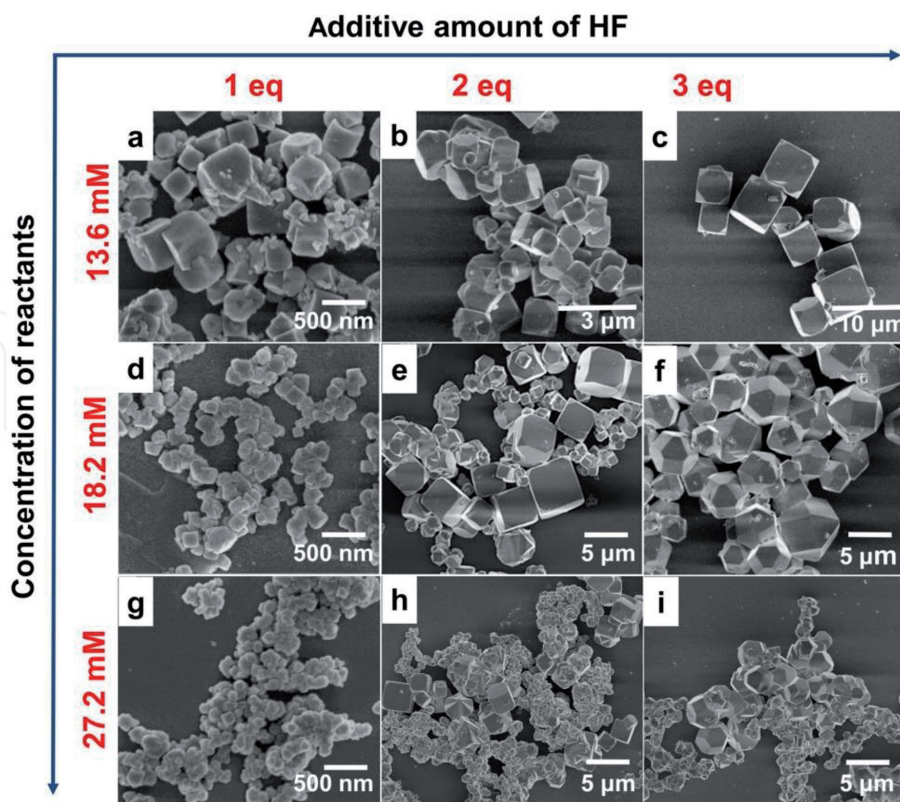

Figure 9.
SEM images of the UiO-66 crystals synthesized with different amounts of HF additive and changing concentrations of the reactants. At $C_{Zr = BDC}$ = 13.6 mM, (a) HF = 1 eq., (b) HF = 2 eq., and (c) HF = 3 eq. At $C_{Zr = BDC}$ = 18.2 mM, (d) HF = 1 eq., (e) HF = 2 eq., and (f) HF = 3 eq. At $C_{Zr = BDC}$ = 27.2 mM, (g) HF = 1 eq., (h) HF = 2 eq., and (i) HF = 3 eq. [47].
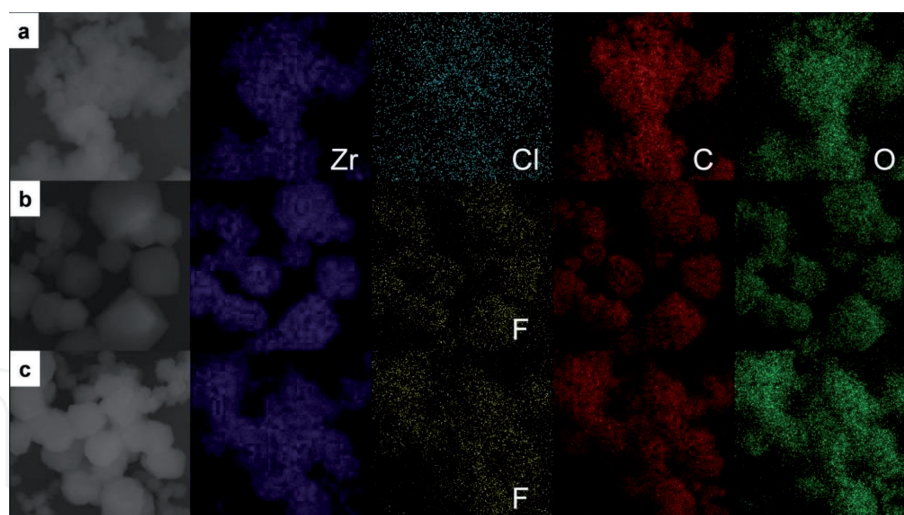
Figure 10.
EDS maps of the UiO-66 crystals synthesized (a) without HF additive, (b) with 3 eq. HF additive, and (c) with 3 eq. HF additive and then heat-treated at 150°C [47].
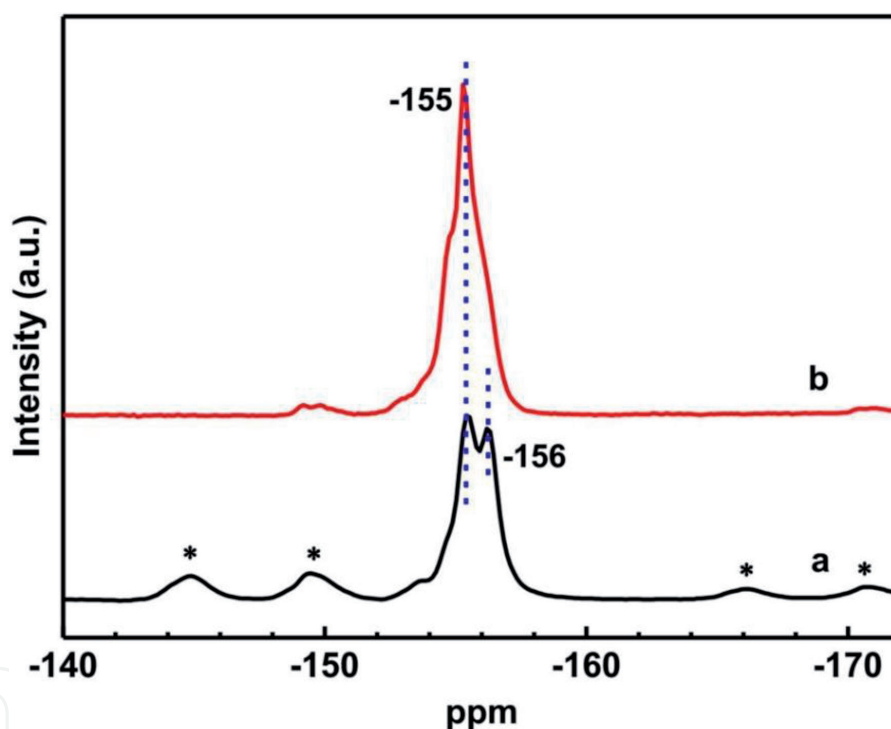

Figure 11.
^{19}F NMR spectra of the 3F-UiO-66 crystals heat-treated at (a) 150°C and (b) 300°C. The asterisks indicate the spinning sidebands [47].

UiO-66 framework. It can be seen that the F introduction has stabilized the framework, as indicated by the progressively increased decomposition temperature. This is attributed to the higher coordination strength of Zr—F in the fluorine-involved crystals than the Zr—Cl or Zr—O in the fluorine-free crystals, resulting in the stabilization of framework structure of the fluorine-involved UiO-66.

Furthermore, as the UiO-66 crystals were modulated from small cube-like morphology to micron-sized cuboctahedron morphology with the addition of the HF during synthesis, their porosity increases [47]. **Figure 13** displays the Ar sorption–desorption isotherms and pore size distributions of the parent and fluorine-involved crystals. As seen, the 3 fluorine-involved crystals (samples c, f, and i in **Figure 9**) exhibit significantly higher Ar adsorption values than the parent crystals
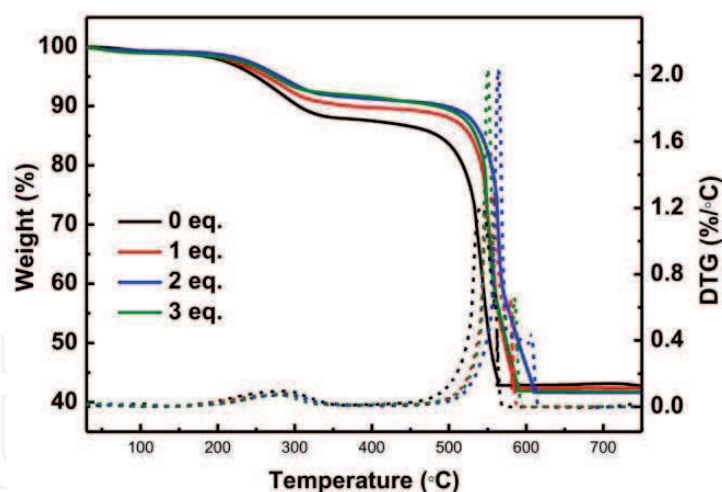
Figure 12.
TGA curves of the UiO-66 crystals synthesized with different amounts of HF additive (C = 18.2 mM) [47].
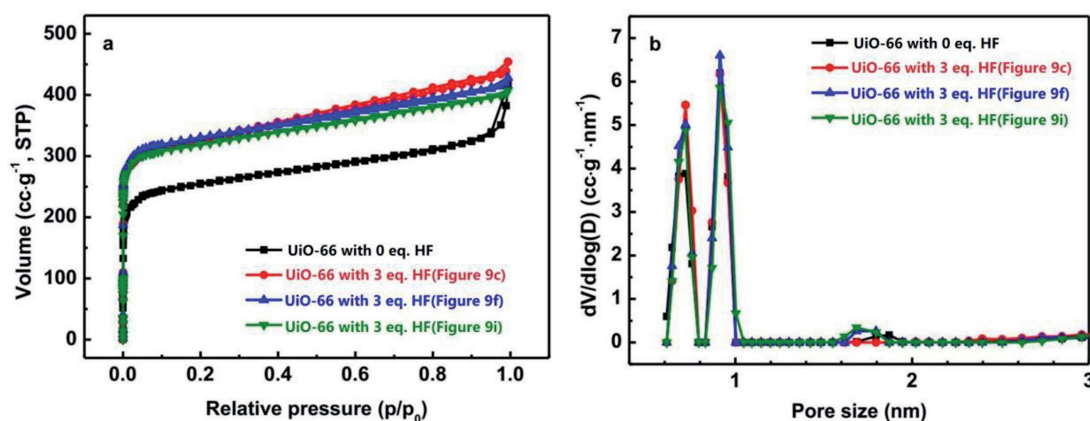

Figure 13.
(a) Ar sorption-desorption isotherms and (b) pore size distributions of the synthesized UiO-66 with various crystal sizes and morphologies [47].

synthesized without HF, and the pore size distributions show the enhanced porosity of the fluorine-involved crystals.

4.3 Modulated synthesis of UiO-66 crystals using solid Cu_2O

In more recent years, nanosized MOFs (also known as nMOFs or NMOFs) have attracted great attentions. nMOFs have short diffusion lengths and high specific surface areas, both are of critical importance in catalysis and sorption, especially in liquid-phase applications [34, 48]. In addition, nMOFs are highly desirable for porous membranes [49, 50], thin film devices [51], and medical applications [52].

We have reported a novel method for the modulated synthesis of nUiO-66 crystals, in which a new type of additive, solid Cu_2O, was used to mediate the synthesis [53]. **Figure 14** shows the TEM images of the UiO-66 crystals synthesized with different amounts of Cu_2O additive. As illustrated, by increasing the amount of Cu_2O additive, the mean sizes of the UiO-66 crystals reduce progressively from ~265 to 40 nm. The crystals maintain an octahedral morphology until when the crystal size is too small to display distinguishable facets and thus appear as spherical particles. The synthesized nano UiO-66 crystals were found to be chemically pure without the contamination of Cu. They have high BET surface area of more than 1100 m^2 g^{-1} and contain rich porosity. **Figure 15** shows the Ar sorption isotherms and pore size distributions of the UiO-66 crystals. Although the amount of micropores
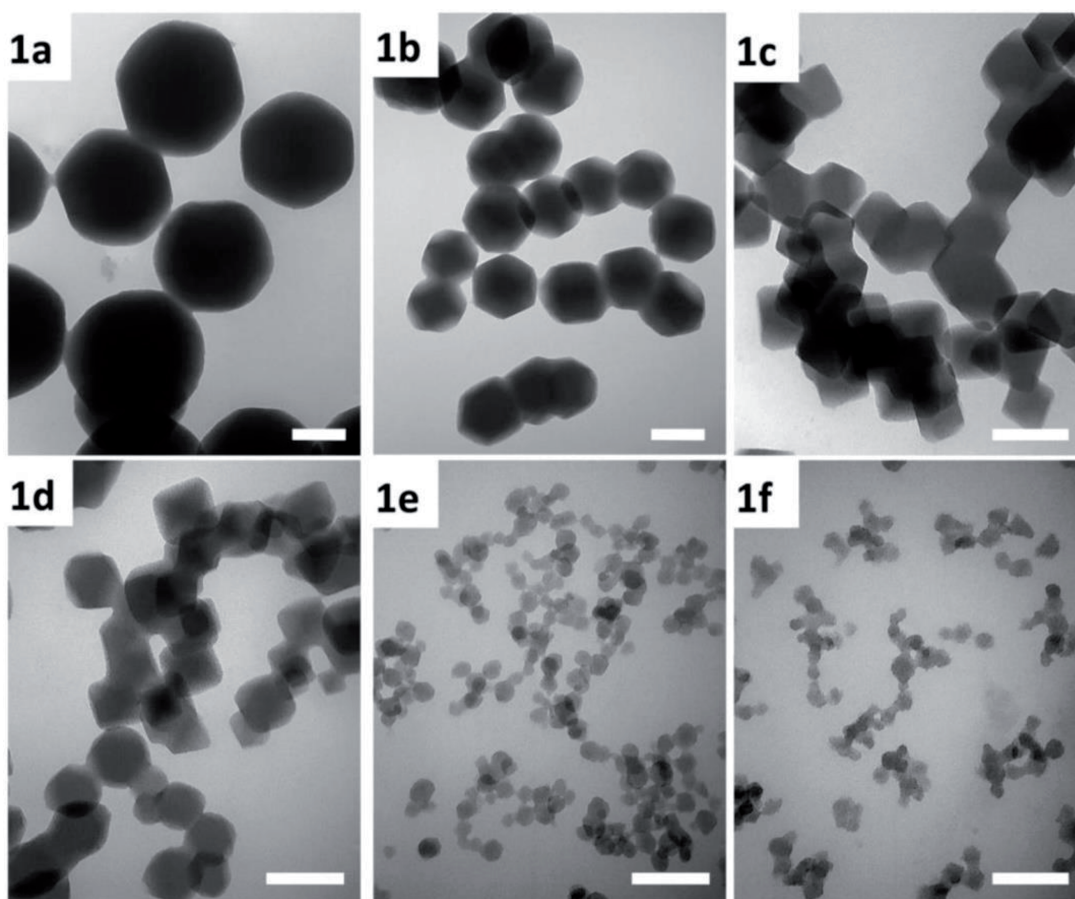
Figure 14.
TEM images of the UiO-66 crystals synthesized with different amounts of Cu$_2$O additive. Here the molar ratio R = n[Cu]/n[ZrCl$_4$]: (1a) R = 0, (1b) R = 0.2, (1c) R = 0.5, (1d) R = 1.0, (1e) R = 1.2, and (1f) R = 1.5. The scale bar is 100 nm [53].
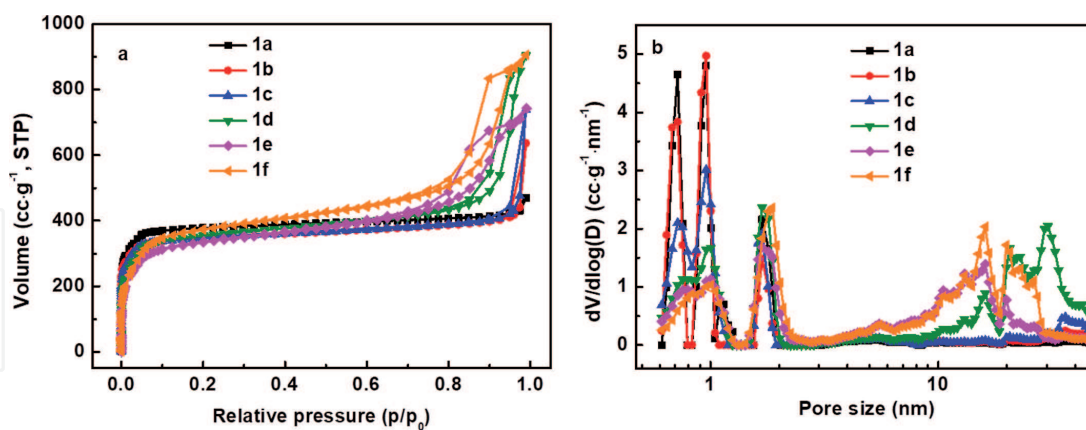

Figure 15.
(a) Ar sorption isotherms and (b) pore size distributions (measured between 0 and 50 nm) of the UiO-66 crystals synthesized with different amounts of Cu$_2$O additive. Here the molar ratio R = n[Cu]/n[ZrCl$_4$]: (1a) R = 0, (1b) R = 0.2, (1c) R = 0.5, (1d) R = 1.0, (1e) R = 1.2, and (1f) R = 1.5 [53].

between 6 Å and 10 Å decreased gradually with the decreasing crystal size, noticeable quantity of mesopores of 10–30 nm became prevailed, demonstrating the dual micro- and mesoporosity of the nano UiO-66 crystals.

During the Cu$_2$O-modulated synthesis, the added solid Cu$_2$O was observed to dissolve gradually in the mother liquor, resulting in the formation of a pale orange-colored solution. **Figure 16** shows the far infrared (FIR) spectra of solid Cu$_2$O and a number of mixed solutions relevant to the synthesis. As illustrated in the inset
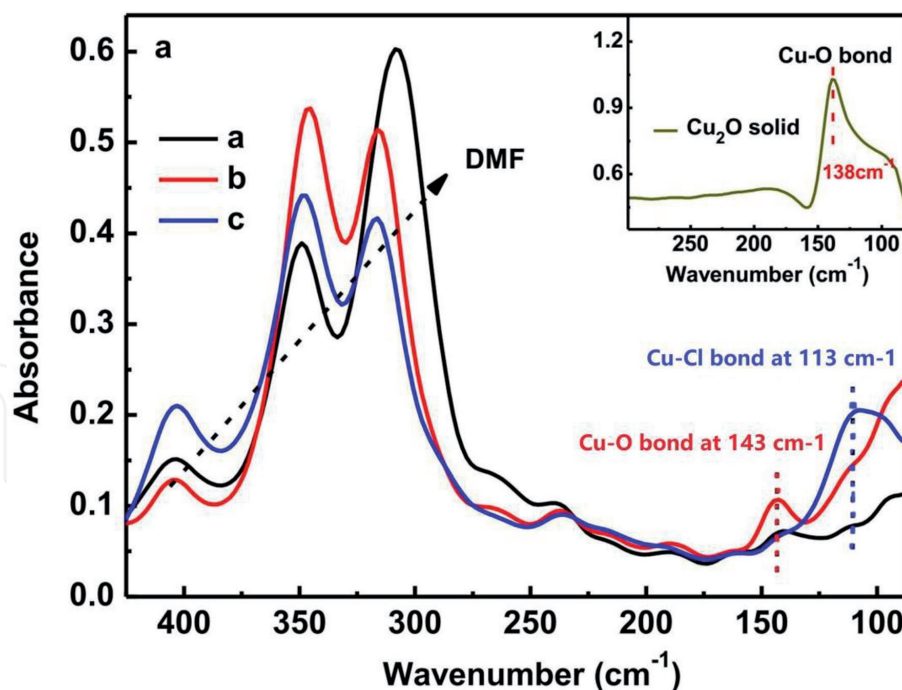
Figure 16.
Far-IR spectra of the solid Cu_2O and a number of mixtures relevant to the UiO-66 synthesis, where the molar ratio of $Cu/ZrCl_4$ is 1.2. (a) $ZrCl_4$/DMF solution, (b) Cu_2O/DMF suspension, and (c) $ZrCl_4$ + Cu_2O/DMF solution. The inset is for solid Cu_2O [53].

of the figure, solid Cu_2O shows the Cu—O absorption band at 138 cm^{-1}. Upon the addition of solid Cu_2O in DMF, the Cu—O bond shifts to 143 cm^{-1} as seen in spectrum b. When the $ZrCl_4$ was added to the suspension of the Cu_2O and DMF, the FIR spectrum (c) shows dramatically decreased Cu—O adsorption band accompanied by the arrival of an intense adsorption band at 113 cm^{-1}. This new band can be ascribed to a shifted stretching vibration of Cu—Cl bonds, which are usually at 109 cm^{-1} for the anionic $[CuCl_2]^-$ complex [54]. The FIR analysis seems to suggest that the dissolution of Cu_2O in the precursor solution of the UiO-66 is driven by the formation of the [Cu—Cl] complexes.

It has also been found [53] that the amount of $ZrCl_4$ in the Cu_2O-modulated synthesis plays a crucial role in the growth of the UiO-66 crystals. The higher the concentration of the $ZrCl_4$, the weaker the Cu_2O's impact on the crystal growth and thus benefits the formation of large size UiO-66 crystals. In contrast, decreasing the concentration of the $ZrCl_4$ favors the production of small UiO-66 crystals, which also accompanied with the loss of crystallinity. It is thus believed that the [Cu—Cl] complex is capable of coordinating with the Zr^{4+}, leading to a decreased coordination of the Zr_6 clusters with BDC linkers, preventing crystal growth.

Additionally, under the modulation of Cu_2O additive, the synthesized UiO-66 crystals not only have reduced sizes, but also enriched structure defects [53]. Both the XRD and TGA analyses of the nano UiO-66 crystals indicate the existence of linker defects and metal cluster defects. **Table 1** presents quantified amounts of the linker missing defects in the synthesized nano UiO-66 crystals. It is seen that the number of linker defects increases with the decreasing crystal size, revealing a more open framework of the nano UiO-66.

In recent years, there have been many reports on the structural defects of the UiO-66 crystals [55–60]. These structural defects are found to relate strongly to the structure stability, adsorption, and catalysts performance of the UiO-66 material.

Sample	Average crystal size of the synthesize nano UiO-66/nm	R	Cu$_2$O addition	
			x	Formula
1a	265	0	0.42	Zr$_6$O$_{6.42}$(BDC)$_{5.58}$
1b	155	0.2	0.50	Zr$_6$O$_{6.50}$(BDC)$_{5.50}$
1c	96	0.5	0.84	Zr$_6$O$_{6.84}$(BDC)$_{5.16}$
1d	75	1.0	0.84	Zr$_6$O$_{6.84}$(BDC)$_{5.16}$
1e	48	1.2	0.84	Zr$_6$O$_{6.84}$(BDC)$_{5.16}$
1f	40	1.5	1.05	Zr$_6$O$_{7.05}$(BDC)$_{4.95}$

Table 1.
Amounts of linker missing defects in the UiO-66 crystals synthesized with the addition of Cu$_2$O [53].

Here R represents the molar ratio of Cu/ZrCl$_4$, and x is the number of linker missing defects. The formula represents the defective molecular formula of the UiO-66 crystals, and Zr$_6$O$_6$(BDC)$_6$ is the formula of a defect-free dehydroxylated UiO-66.

4.4 In situ synthesis of Ti-doped hybrid UiO-66 crystals

Introducing foreign metal centres into the framework structure to obtain hybrid (i.e. mixed metal) MOFs is a strategy for developing novel MOFs. We have explored the possibility of facile synthesis of Ti^{4+}-doped hybrid UiO-66-nTi MOFs via an in situ crystallization process [61]. In this work, a series of Ti^{4+}-doped UiO-66-nTi (n represents the mass fraction of Ti^{4+}) crystals were synthesized following the synthesis procedure of the UiO-66, but with the addition of varying amounts of Ti^{4+} in the
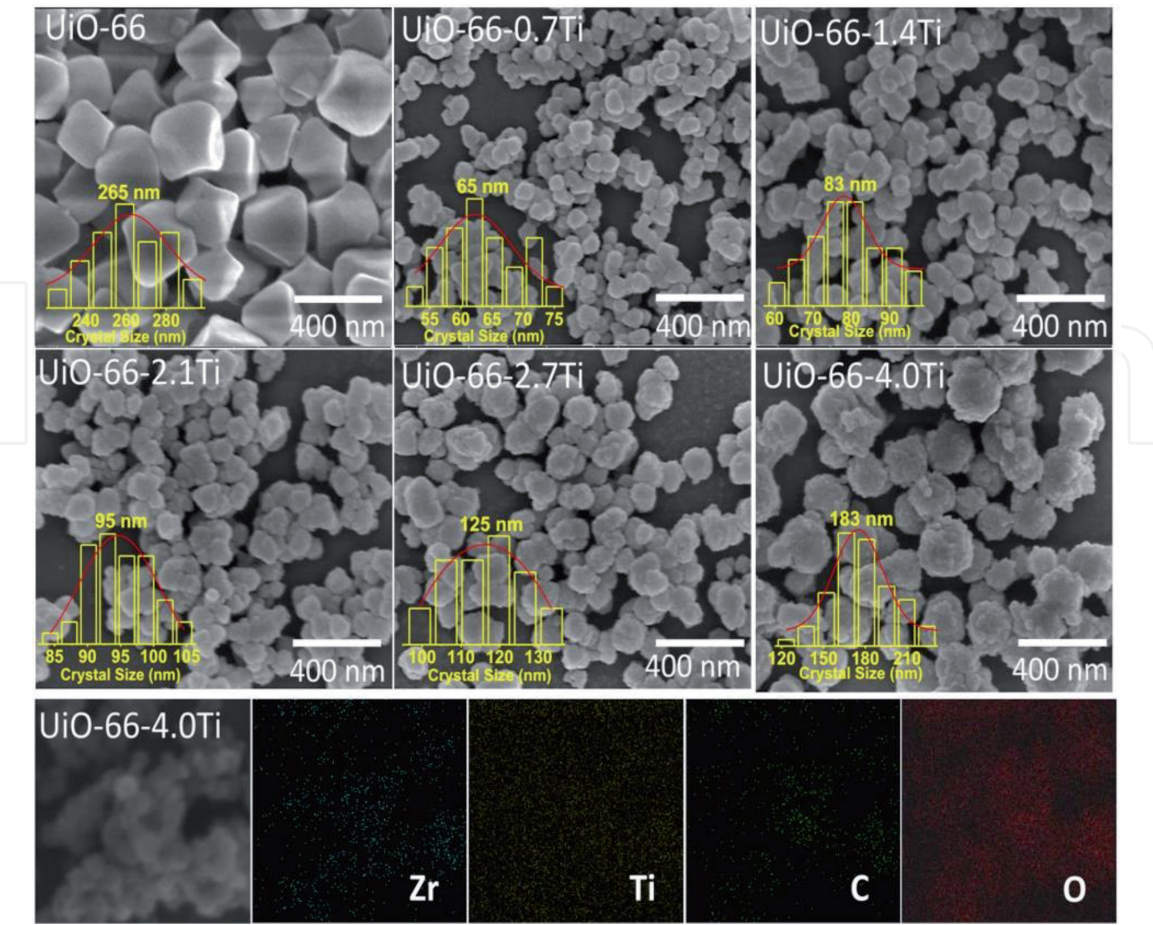

Figure 17.
SEM images of the UiO-66-nTi MOFs and EDS elemental mappings of UiO-66-4Ti [61].

form of titanium isopropoxide in the precursor solution. The ICP analysis showed that the concentration of Ti^{4+} increases gradually from around 0.7 to 4.0 wt% in the resulted crystals with increased addition of Ti^{4+} in the synthesis.

Figure 17 shows the SEM images and EDS elemental mapping of the synthesized UiO-66-*n*Ti crystals. It is evident that there is a significant difference on the crystal morphology and size of the UiO-66 crystals as the result of Ti^{4+} doping. The parent UiO-66 contains octahedral crystals of a mean size ~265 nm. With increased Ti^{4+} doping concentration, the UiO-66-*n*Ti crystals change from octahedrons to sphere-like crystals with rougher facets, and their mean crystal sizes decrease sharply from 265 to ~65 nm. This seems to suggest that the doping of Ti^{4+} restraints the growth of the UiO-66-*n*Ti crystals. It is noteworthy that when the Ti^{4+} concentration was further increased, the UiO-66-*n*Ti crystals maintain the sphere-like morphology, but the mean size increases from 65 to 183 nm, unexpectedly.

Figure 18 shows the FT-IR spectra of the parent UiO-66 and doped UiO-66-*n*Ti crystals. As seen, for the parent UiO-66, the Zr—$O_{\mu3\text{-}O}$ stretch in the [Zr—O] clusters is observed at ~682 cm^{-1}, moving towards 664 cm^{-1} with the increase in the Ti^{4+} doping amounts, indicating the structural change in the Ti^{4+}-doped UiO-66-*n*Ti crystals. As reported in the literatures [32, 62], the MIL-125(Ti) and NH_2-MIL-125(Ti) MOFs are built from coordination between Ti_8 clusters and H_2BDC-type organic linkers. Both structures display a FT-IR band at between 600 and 700 cm^{-1} which resulted from (O—Ti—O) vibrations, and for the NH_2-MIL-125(Ti), the (O—Ti—O) vibrations occur at ~642 cm^{-1}. We thus believe that the red shift of the Zr—$O_{\mu3\text{-}O}$ stretch in the UiO-66-*n*Ti crystals could be caused by the incorporation of the Ti^{4+} in the [Zr—O] clusters.

Figure 19 shows the EXAFS spectra of the parent UiO-66 and doped UiO-66-2.7Ti crystals. It further demonstrates the alternation in coordination state around the Zr^{4+} caused by the Ti^{4+} doping. As seen, the peak at ~1.7 Å that relates to the Zr—O bonds shifts to 1.6 Å after Ti^{4+} doping. Additionally, the peak at around 3.0 Å

Figure 18.
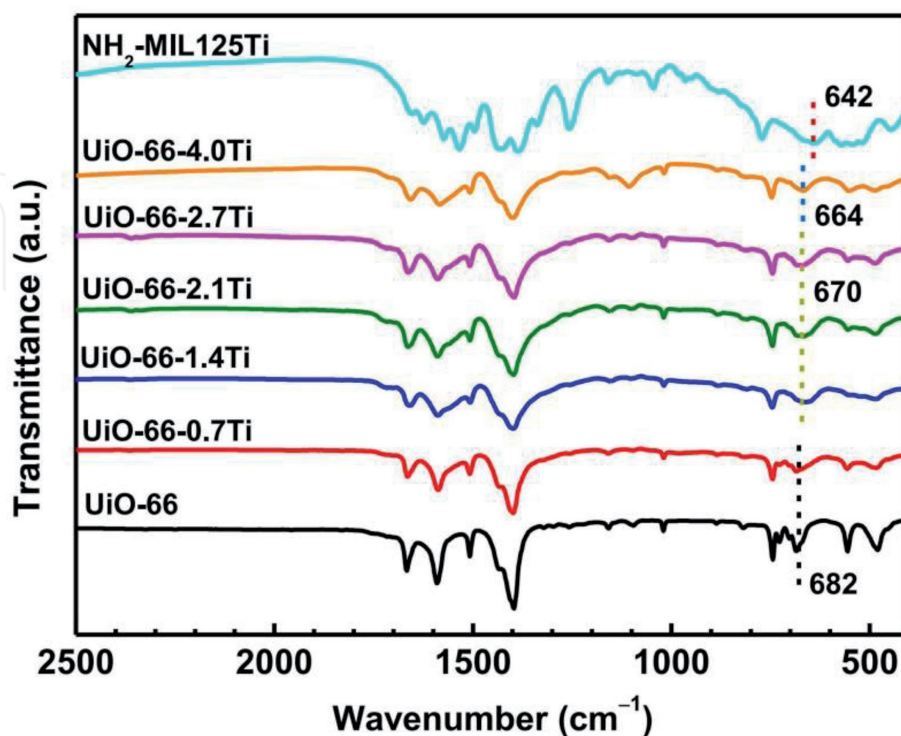*FT-IR spectra of the parent UiO-66, doped UiO-66-*n*Ti (n = 0.7, 1.4, 2.1, 2.7, and 4.0), and NH₂-MIL-125(Ti) crystals [61].*
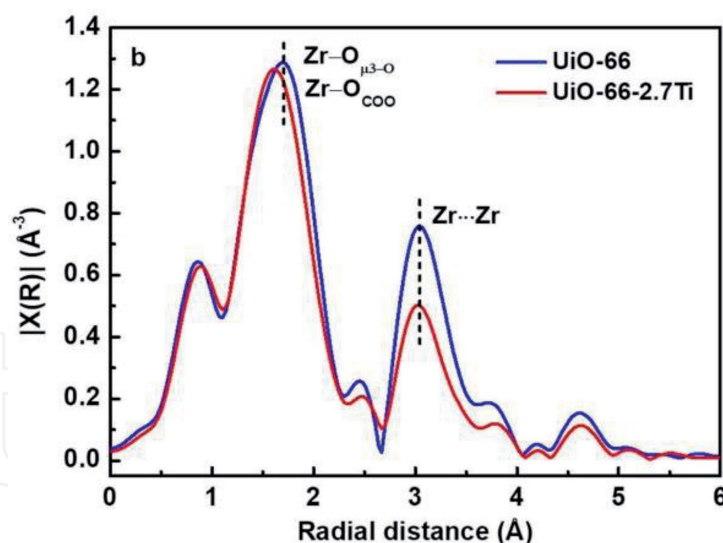
Figure 19.
EXAFS spectra of the parent UiO-66 and the UiO-66-2.7Ti crystals [61].

that represents the Zr···Zr bonds connecting through the $O_{\mu3\text{-}O}$ or $O_{\mu3\text{-}OH}$ decreases noticeably after doping, likely due to the formation of Zr···Ti coordination.

The synthesized UiO-66-*n*Ti crystals have been found to be highly selective and efficient in removing anionic dye, the Congo red, from water. The doped UiO-66-2.7Ti (i.e. with 2.72 wt% Ti^{4+} incorporation) exhibited the highest adsorption capacity of 979 mg g^{-1}, 3.6 times of the parent UiO-66 crystals.

5. Conclusions

MOFs, with their inherent high surface areas, uniform, versatile, and tuneable pores, and tailorable physicochemical properties, have been projected to have a broad range of potential applications in various areas. Since the discovery of the first MOF structure in the 1990s, hundreds of new MOFs have been synthesized successfully.

In the past two decades, much attention has been paid to develop methods to control the morphology and size of MOF crystals, in order to tailor the structure properties and performance of MOF materials. Such research efforts have resulted in the development of effective synthesis methods which are capable of modulation of morphology and size of MOF crystals through different mechanisms, including the deprotonation regulation, coordination modulation, and surfactant modulation synthesis. This review chapter has highlighted a number of successful synthesis routes using, for example, the carboxylic acids, HF, and solid Cu_2O additives to modulate the MOF crystal formation and growth. It has also demonstrated the ability of doping to create hybrid MOFs with improved properties and functionalities.

It remains a significant challenge on how to best fully utilize the unique set of properties and functionalities of the chemically versatile MOFs and realize their application potentials in various identified areas. While there have been significant achievements on the structure optimization and performance development of MOFs to date, it is anticipated that further progress can be made with more fundamental research and industrial application of MOFs.

Acknowledgements

Author details

Yitong Han[1,2], Hong Yang[3] and Xinwen Guo[2*]

1 Dalian Research Institute of Petroleum and Petrochemicals, SINOPEC, Dalian, China

2 State Key Laboratory of Fine Chemicals, PSU-DUT Joint Centre for Energy Research, School of Chemical Engineering, Dalian University of Technology, Dalian, China

3 Department of Mechanical Engineering (M050), The University of Western Australia, Perth, WA, Australia

*Address all correspondence to: guoxw@dlut.edu.cn

IntechOpen

References

[1] Sing KS. Reporting physisorption data for gas/solid systems with special reference to the determination of surface area and porosity (recommendations 1984). Pure and Applied Chemistry. 1985;**57**:603-619

[2] Cundy CS, Cox PA. The hydrothermal synthesis of zeolites: History and development from the earliest days to the present time. Chemical Reviews. 2003;**103**:663-701

[3] Xia YD, Yang ZX, Zhu YQ. Porous carbon-based materials for hydrogen storage: Advancement and challenges. Journal of Materials Chemistry A. 2013;**1**:9365-9381

[4] Wales DJ, Grand J, Ting VP, Burke RD, Edler KJ, Bowen CR, et al. Gas sensing using porous materials for automotive applications. Chemical Society Review. 2015;**44**:4290-4321

[5] Sun MH, Huang SZ, Chen LH, Li Y, Yang XY, Yuan ZY, et al. Applications of hierarchically structured porous materials from energy storage and conversion, catalysis, photocatalysis, adsorption, separation, and sensing to biomedicine. Chemical Society Review. 2016;**45**:3479-3563

[6] Chen YQ, Chen KW, Bai H, Li L. Electrochemically reduced graphene porous material as light absorber for light-driven thermoelectric generator. Journal of Materials Chemistry. 2012;**22**:17800-17804

[7] Wang BJ, Prinsen P, Wang HZ, Bai ZS, Wang HL, Luque R, et al. Macroporous materials: Microfluidic fabrication, functionalization and applications. Chemical Society Review. 2017;**46**:855-914

[8] Kitagawa S, Kitaura R, Noro S. Functional porous coordination polymers. Angewandte Chemie, International Edition. 2004;**43**:2334-2375

[9] Ockwig NW, Delgado-Friedrichs O, O'keeffe M, Yaghi OM. Reticular chemistry: Occurrence and taxonomy of nets and grammar for the design of frameworks. Accounts of Chemical Research. 2005;**38**:176-182

[10] Zhu QL, Xu Q. Metal-organic framework composites. Chemical Society Review. 2014;**43**:5468-5512

[11] Jia JH, Lin X, Wilson C, Blake AJ, Champness NR, Hubberstey P, et al. Twelve-connected porous metal-organic frameworks with high H_2 adsorption. Chemical Communications. 2007;**8**:840-842

[12] Rosi NL, Eckert J, Eddaoudi M, Vodak DT, Kim J, O'Keeffe M, et al. Hydrogen storage in microporous metal-organic frameworks. Science. 2003;**300**:1127-1129

[13] Férey G, Mellot-Draznieks C, Serre C, Millange F, Dutour J, Surblé S, et al. A chromium terephthalate-based solid with unusually large pore volumes and surface area. Science. 2005;**309**:2040-2042

[14] Furukawa H, Cordova KE, O'Keeffe M, Yaghi OM. The chemistry and applications of metal-organic frameworks. Science. 2013;**341**:1230444

[15] Queen WL, Brown CM, Britt DK, Zajdel P, Hudson MR, Yaghi OM. Site-specific CO_2 adsorption and zero thermal expansion in an anisotropic pore network. Journal of Physical Chemistry C. 2011;**115**:24915-24919

[16] Xue DX, Belmabkhout Y, Shekhah O, Jiang H, Adil K, Cairns AJ, et al. Tunable rare earth Fcu-MOF platform: Access to adsorption kinetics driven gas/vapor separations via pore

size contraction. Journal of American Chemical Society. 2015;**137**:5034-5040

[17] Belmabkhout Y, Guillerm V, Eddaoudi M. Low concentration CO_2 capture using physical adsorbents: Are metal–organic frameworks becoming the new benchmark materials? Chemical Engineering Journal. 2016;**296**:386-397

[18] Øien-Ødegaard S, Bouchevreau B, Hylland K, Wu LP, Blom R, Grande C, et al. UiO-67-type metal-organic frameworks with enhanced water stability and methane adsorption capacity. Inorganic Chemistry. 2016;**55**:1986-1991

[19] Guo YX, Feng X, Han TY, Wang S, Lin ZG, Dong YP, et al. Tuning the luminescence of metal-organic frameworks for detection of energetic heterocyclic compounds. Journal of American Chemical Society. 2014;**136**:15485-15488

[20] Nickerl G, Senkovska I, Kaskel S. Tetrazine functionalized zirconium MOF as an optical sensor for oxidizing gases. Chemical Communications. 2015;**51**:2280-2282

[21] Yang XQ, Yan DP. Long-afterglow metal-organic frameworks: Reversible guest-induced phosphorescence tunability. Chemical Science. 2016;**7**:4519-4526

[22] Pentyala V, Davydovskaya P, Ade M, Pohle R, Urban G. Metal-organic frameworks for alcohol gas sensor. Sensors and Actuators B. 2016;**222**:904-909

[23] Wu XL, Yang C, Ge J, Liu Z. Polydopamine tethered enzyme/metal-organic framework composites with high stability and reusability. Nanoscale. 2015;**7**:18883-18886

[24] Choi KM, Na K, Somorjai GA, Yaghi OM. Chemical environment control and enhanced catalytic performance of platinum nanoparticles embedded in nanocrystalline metal-organic frameworks. Journal of American Chemical Society. 2015;**137**:7810-7816

[25] Carson F, Martínez-Castro E, Marcos R, Miera GG, Jansson K, Zou XD, et al. Effect of the functionalisation route on a Zr-MOF with an Ir-NHC complex for catalysis. Chemical Communications. 2015;**51**:10864-10867

[26] Yamada T, Otsubo K, Makiura R, Kitagawa H. Designer coordination polymers: Dimensional crossover architectures and proton conduction. Chemical Society Reviews. 2013;**42**:6655-6669

[27] Liu JX, Zhou WC, Liu JX, Howard I, Kilibarda G, Schlabach S, et al. Photoinduced charge-carrier generation in epitaxial MOF thin films: High efficiency as a result of an indirect electronic band gap? Angewandte Chemie International Edition. 2015;**54**:7441-7445

[28] Bao T, Zhang J, Zhang WP, Chen ZL. Growth of metal-organic framework HKUST-1 in capillary using liquid-phase epitaxy for open-tubular capillary electrochromatography and capillary liquid chromatography. Journal of Chromatography A. 2015;**1381**:239-246

[29] Qiu S, Xue M, Zhu GS. Metal-organic framework membranes: From synthesis to separation application. Chemical Society Reviews. 2014;**43**:6116-6140

[30] Rubio-Martinez M, Avci-Camur C, Thornton AW, Imaz I, Maspoch D, Hill MR. New synthetic routes towards MOF production at scale. Chemical Society Review. 2017;**46**:3453-3480

[31] Tao AR, Habas S, Yang PD. Shape control of colloidal metal nanocrystals. Small. 2008;**4**:310-325

[32] Hu S, Liu M, Li KY, Zou Y, Zhang AF, Song CS, et al. Solvothermal synthesis of NH$_2$-MIL-125(Ti) from circular plate to octahedron. CrystEngComm. 2014;**16**:9645-9650

[33] Zahn G, Zerner P, Lippke J, Kempf FL, Lilienthal S, Schröder CA, et al. Insight into the mechanism of modulated syntheses: In situ synchrotron diffraction studies on the formation of Zr-Fumarate MOF. CrystEngComm. 2014;**16**:9198-9207

[34] Tsuruoka T, Furukawa S, Takashima Y, Yoshida K, Isoda S, Kitagawa S. Nanoporous nanorods fabricated by coordination modulation and oriented attachment growth. Angewandte Chemie, International Edition. 2009;**48**:4739-4743

[35] Diring S, Furukawa S, Takashima Y, Tsuruoka T, Kitagawa S. Controlled multiscale synthesis of porous coordination polymer in nano/micro regimes. Chemistry of Materials. 2010;**22**:4531-4538

[36] Umemura A, Diring S, Furukawa S, Uehara H, Tsuruoka T, Kitagawa S. Morphology design of porous coordination polymer crystals by coordination modulation. Journal of the American Chemical Society. 2011;**133**:15506-15513

[37] Jiang DM, Mallat T, Krumeich F, Baiker A. Polymer-assisted synthesis of nanocrystalline copper-based metal-organic framework for amine oxidation. Catalysis Communications. 2011;**12**:602-605

[38] Cai XC, Lin J, Pang ML. Facile synthesis of highly uniform Fe-MIL-88B particles. Crystal Growth & Design. 2016;**16**:3565-3568

[39] Yang JM, Qi ZP, Kang YS. Effect of additives on morphology and size and gas adsorption of SUMOF-3 microcrystals. Microporous and Mesoporous Materials. 2016;**222**:27-32

[40] Li WH, Zhang AF, Jiang X, Chen C, Liu ZM, Song CS, et al. Low temperature CO$_2$ methanation: ZIF-67-derived co-based porous carbon catalysts with controlled crystal morphology and size. ACS Sustainable Chemical Engineer. 2017;**5**:7824-7831

[41] Ma MY, Zacher D, Zhang XN, Fisher RA, Metzler-Nolte NA. Method for the preparation of highly porous, nanosized crystals of isoreticular metal-organic frameworks. Crystal Growth & Design. 2011;**11**:185-189

[42] Yang JM, Liu Q, Kang YS. Controlled growth and gas sorption properties of IRMOF-3 nano/microcrystals. Dalton Transactions. 2014;**43**:16707-16712

[43] Liu Q, Jin LN, Facile Fabrication SWY. Adsorption property of a nano/microporous coordination polymer with controllable size and morphology. Chemical Communication. 2012;**48**:8814-8816

[44] Pan YC, Heryadi D, Zhou F, Zhao L, Lestari G, Su HB, et al. Tuning the crystal morphology and size of zeolitic imidazolate framework-8 in aqueous solution by surfactants. CrystEngComm. 2011;**13**:6937-6940

[45] Cavka JH, Jakobsen S, Olsbye U, Guillou N, Lamberti C, Bordiga S, et al. A new zirconium inorganic building brick forming metal organic frameworks with exceptional stability. Journal of the American Chemical Society. 2008;**130**:13850-13851

[46] Schaate A, Roy P, Godt A, Lippke J, Waltz F, Wiebcke M, et al. Modulated synthesis of Zr-based metal-organic frameworks: From nano to single

crystals. Chemistry— A European Journal. 2011;**17**:6643-6651

[47] Han YT, Liu M, Li KY, Zuo Y, Wei YX, Xu ST, et al. Facile synthesis of morphology and size-controlled zirconium metal-organic framework UiO-66: The role of hydrofluoric acid in crystallization. CrystEngComm. 2015;**17**:6434-6440

[48] Díaz-García M, Mayoral Á, Díaz I, Sánchez-Sánchez M. Nanoscaled M-MOF-74 materials prepared at room temperature. Crystal Growth & Design. 2014;**14**:2479-2487

[49] Huang AS, Wang NY, Caro J. Seeding-free synthesis of dense zeolite FAU membranes on 3-aminopropyltriethoxysilane-functionalized alumina supports. Journal of Membrane Science. 2012;**389**:272-279

[50] Mao YY, Cao W, Li JW, Sun LW, Peng XS. HKUST-1 membranes anchored on porous substrate by hetero MIL-110 nanorod array seeds. Chemistry— A European Journal. 2013;**19**:11883-11886

[51] Stassen I, Campagnol N, Fransaer J, Vereecken P, Vos DD, Ameloot R. Solvent-free synthesis of supported ZIF-8 films and patterns through transformation of deposited zinc oxide precursors. CrystEngComm. 2013;**15**:9308-9311

[52] deKrafft KE, Boyle WS, Burk LM, Zhou OZ, Lin WB. Zr- and Hf-based nanoscale metal-organic frameworks as contrast agents for computed tomography. Journal of Materials Chemistry. 2012;**22**:18139-18144

[53] Han YT, Liu M, Li KY, Sun Q, Song CS, Zhang GL, et al. Cu_2O mediated synthesis of metal-organic framework UiO-66 in nanometer scale. Crystal Growth & Design. 2017;**17**:685-692

[54] Nakamoto K. Infrared and Raman Spectra of Inorganic and Coordination Compounds. 3rd ed. New York: Wiley; 1978. pp. 115-137

[55] Fang ZL, Bueken B, Vos DED, Fischer RA. Defect-engineered metal–organic frameworks. Angewandte Chemie, International Edition. 2015;**54**:7234-7254

[56] Vandichel M, Hajek J, Ghysels A, Vos AD, Waroquier M, Speybroeck VV. Water coordination and dehydration processes in defective UiO-66 type metal organic frameworks. CrystEngComm. 2016;**18**:7056-7069

[57] Shearer GC, Chavan S, Bordiga S, Svelle S, Olsbye U, Lillerud KP. Defect engineering: Tuning the porosity and composition of the metal-organic framework UiO-66 via modulated synthesis. Chemistry of Materials. 2016;**28**:3749-3761

[58] Vandichel M, Hajek J, Vermoortele F, Waroquier M, Vos DED, Speybroeck V. Active site engineering in UiO-66 type metal–organic frameworks by intentional creation of defects: A theoretical rationalization. CrystEngComm. 2015;**17**:395-406

[59] Thornton AW, Babarao R, Jain A, Trousselet F, Coudert FX. Defects in metal-organic frameworks: A compromise between adsorption and stability? Dalton Transactions. 2016;**45**:4352-4359

[60] Canivet J, Vandichel M, Farrusseng D. Origin of highly active metal-organic frameworks catalysts: Defects? Defects! Dalton Transactions. 2016;**45**:4090-4099

[61] Han YT, Liu M, Li KY, Sun Q, Zhang WS, Song CS, et al. In situ synthesis of titanium doped hybrid metal-organic framework UiO-66 with enhanced adsorption capacity

for organic dyes. Inorganic Chemistry
Frontiers. 2017;**4**:1870-1880

[62] Dan-Hardi M, Serre C, Frot T,
Rozes L. A new photoactive crystalline
highly porous titanium (IV)
dicarboxylate. Journal of the American
Chemical Society. 2009;**131**:10857-10859